Chemical Science

ROYAL SOCIETY OF CHEMISTRY

EDGE ARTICLE

View Article Online
View Journal | View Issue

Cite this: *Chem. Sci.*, 2023, **14**, 2123

All publication charges for this article have been paid for by the Royal Society of Chemistry

Received 17th November 2022
Accepted 23rd January 2023

DOI: 10.1039/d2sc06342e

rsc.li/chemical-science

A biocompatible and fully erodible conducting polymer enables implanted rechargeable Zn batteries†

Xiaoteng Jia,[a] Xuenan Ma,[a] Li Zhao,[a] Meiying Xin,[b] Yulei Hao,[b] Peng Sun,[a] Chenguang Wang,[a] Danming Chao,[d] Fangmeng Liu,*[a] Caiyun Wang,*[c] Geyu Lu*[ae] and Gordon Wallace[c]

Implanted rechargeable batteries that can provide energy over a sufficient lifetime and ultimately degrade into non-toxic byproducts are highly desirable. However, their advancement is significantly impeded by the limited toolbox of electrode materials with a known biodegradation profile and high cycling stability. Here we report biocompatible, erodible poly(3,4-ethylenedioxythiophene) (PEDOT) grafted with hydrolyzable carboxylic acid pendants. This molecular arrangement combines the pseudocapacitive charge storage from the conjugated backbones and dissolution *via* hydrolyzable side chains. It demonstrates complete erosion under aqueous conditions in a pH-dependent manner with a predetermined lifetime. The compact rechargeable Zn battery with a gel electrolyte offers a specific capacity of 31.8 mA h g^{-1} (57% of theoretical capacity) and outstanding cycling stability (78% capacity retention over 4000 cycles at 0.5 A g^{-1}). Subcutaneous implantation of this Zn battery into Sprague-Dawley (SD) rats demonstrates complete biodegradation *in vivo* and biocompatibility. This molecular engineering strategy presents a viable avenue for developing implantable conducting polymers with a predetermined degradation profile and high energy storage capability.

Introduction

Biodegradable implantable medical bionics have gained exposure from biomedicine to microelectromechanical systems.[1,2] A biocompatible and biodegradable power source with predictable performance over the service time is highly desirable to drive these bionics. An on-board battery provides a feasible solution because of the attainable high energy density and reliable operation.[3,4]

Galvanic cells consisting of bioresorbable metals (*e.g.* Mg, Zn, Fe, Mo, and their alloys) have demonstrated utility in ingestible diagnostics.[5,6] However, these primary batteries with short lifetimes (from hours to weeks) hinder the mid-term operation *in vivo*. Implanted rechargeable batteries that can sustain long-term cyclic use are preferred. Biologically derived redox-active biopolymers, such as melanin pigments, dopamine, and nicotinamide adenine dinucleotide cofactor, can be recharged *in vivo*.[7,8] However, the lack of precise control over the biodegradation kinetics of these endogenous redox organics stemming from the complicated molecular structures may lead to undesirable biological responses. An inorganic intercalation material is also challenging in this case due to inferior electronic conductivity and sluggish ionic diffusion, leading to unfavorable rate capability and cycling stability.[9] Therefore, alternative approaches are necessary to expand the toolbox for biocompatible energy storage materials with both desired electrochemical properties (*e.g.* high energy density, rate capacity, and cycling stability) and programmable biodegradable profiles under physiological conditions.[10]

Conducting polymers have demonstrated applicability as high-rate electrode materials attributed to pseudocapacitive-dominant energy storage behavior. They offer tunable charge storage, electronic, and degradation properties through molecular design.[11] However, imparting both full biodegradation and electroactivity to conducting polymers represents a formidable challenge because of the limited cleavable linkages that could maintain extended conjugation along the backbone.[12] The formed polymer composite from blending or covalent bonding with biodegradable polyesters, polyamides, and polyanhydrides[13] can only be disintegrated leaving the active components in the body. These materials can only be disintegrated without complete chemical breakdown, leaving the active components in the body. To eliminate the

[a]*State Key Laboratory of Integrated Optoelectronics, College of Electronic Science and Engineering, Jilin University, Changchun 130012, China. E-mail: liufangmeng@jlu.edu.cn; lugy@jlu.edu.cn*

[b]*Jilin Provincial Key Laboratory of Pediatric Neurology, Department of Pediatric Neurology, The First Hospital of Jilin University, 130021, China*

[c]*ARC Centre of Excellence for Electromaterials Science, Intelligent Polymer Research Institute, AIIM Faculty, University of Wollongong, Wollongong, NSW 2522, Australia. E-mail: caiyun@uow.edu.au*

[d]*College of Chemistry, Jilin University, Changchun 130012, China*

[e]*International Center of Future Science, Jilin University, Changchun 130012, China*

† Electronic supplementary information (ESI) available: Experimental electrochemical performance comparison of biodegradable implanted batteries, synthesis, and characterization of monomers and polymers. See DOI: https://doi.org/10.1039/d2sc06342e

undesired immune response caused by the undegraded active components, Bao and coworkers designed fully biodegradable semiconducting polymers for transient electronics by incorporating a reversible acid-labile imine bond into a diketopyrrolopyrrole-based polymer, where imine hydrolysis resulted in the cleavage of the polymer backbone.[14,15] They further investigated the impact of side chains on the degradation lifetimes in different solvents.[16] However, the hydrolytic cleavage chemistry along the polymer mainchain represents a particular challenge in maintaining the conjugation length, *i.e.* energy storage capacity. Moreover, the low electrical conductivity of these conjugated polymers significantly limits the practical application in batteries, where fast rechargeability and high cycling stability are highly desirable. A rationally tailored biodegradable conducting polymer with full biodegradation and high cycling stability is urgently needed to realize biodegradable rechargeable batteries.

Here, we present a biocompatible, fully erodible PEDOT derivative by adopting bio-resorption chemistry (Fig. 1) *via* both chemical and electrochemical routes. Covalent tethering of PEDOT with sulfonate and carboxyl groups endows the polymer with water solubility and wet-processing capability.[17] To control the bioerosion rate, an ether spacer was linked to the acid group to decrease water solubility.[18] Compared with the hydrolytically cleavable linkages at the polymer mainchain, side-chain engineering of ionizable and/or hydrolyzable carboxylic acid pendants concurrently allows for charge storage and modulation of dissolution kinetics without compromising electronic properties.[19] The electropolymerized film, eliminating the need for conductive additives, delivers a high capacity, outstanding rate, and cycling performance when coupled with a Zn anode. This battery demonstrates complete disappearance *in vivo* through a series of metabolic and hydrolytic reactions, and its biocompatibility is evidenced by live–dead cell imaging and histological analysis. This work provides a new avenue for molecular engineering of biocompatible and fully erodible conducting polymers for an onboard energy supply.

Results and discussion

Synthesis of PEDOT–COOH

Carboxylic acid-functionalized EDOT (EDOT–COOH) was obtained by direct esterification of EDOT–OH in the presence of NaH and subsequently treated with NaOH (Fig. S1a†).[17] A colloidal dispersion of PEDOT–COOH was obtained by $FeCl_3$ mediated chemical polymerization of the monomer, followed by deprotonation in NaOH solution. Direct electropolymerization of PEDOT–COOH was also achieved using cyclic voltammetry induced oxidation to deposit the polymer onto a gold leaf substrate, which was imprinted onto polyvinyl alcohol (PVA) sheets (Fig. S1b†). The oxidation current grew after the first cycle, accompanied by an anodic shift, indicating polymer chain growth. The electropolymerized film on the PVA–Au substrate could be used directly as a biodegradable electrode. The proton signal at 12.1 ppm from ^{1}H NMR confirmed the incorporation of the carbonyl group into the polymer backbone (Fig. S2 and S3†). The absorption spectra of PEDOT–COOH in dimethyl sulfoxide (DMSO) revealed a broad absorption band centered at around 530 nm, corresponding to the π–π^* transition in the conjugated backbone (Fig. S4†). PEDOT–COOH was sparingly soluble in DMSO (1 wt%), water (~0.2 wt%), and basic aqueous solutions (10 wt%, pH 12) at room temperature.

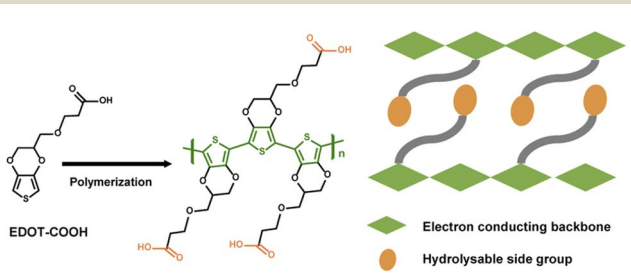

Fig. 1 Chemical structures and structural functionalities of erodible PEDOT–COOH.

Bioerosion and cytocompatibility of PEDOT–COOH

Given the low water solubility, we hypothesized that PEDOT–COOH might undergo a gradual erosion/dissolution process under physiological conditions in a manner similar to bio-erodible polymers.[20,21] Unlike conventional biodegradable polymers, whose polymer backbone is partial/fully degraded into monomeric units, bio-erodible polymers can be dissolved away in aqueous environments with a molecular weight suitable for renal filtration (30–50 kDa).[17] To test this hypothesis, electropolymerized PEDOT–COOH films were incubated in different pH phosphate-buffered saline (PBS) buffers at 37 °C. Thin films deposited on ITO dissolved within 24 hours at pH 10, but dissolved more slowly at pH 4. Intermediate dissolution rates were observed at pH 7.4.

To quantitatively analyze the bioerosion profile, we incubated the pellets of chemically polymerized PEDOT–COOH (30 mg, 10 mm diameter and 0.5 mm thickness) in buffers of varying pH. The solution was changed every 12 h and monitored using UV-Vis spectroscopy. The erosion rate was dramatically enhanced as pH increased with complete dissolution after 7 days at pH 7.4 and 4 days at pH 10 (Fig. 2a). This erosion rate was much higher than previously reported for bio-erodible polypyrrole (PPy) with the carboxylic acid group (27% weight loss after 80 days of incubation in pH 7.2 buffer) attributed to the hydrophilicity and polarity of ether side-chains.[22] However, the weight loss was only 16% after 7 days of incubation in pH 4 buffer due to the inhibition of carboxyl hydrolysis under acidic conditions. The mass loss results coincided with the increased absorption at $\lambda = 350$ nm in the PBS solution (Fig. 2b). The main absorption peak at 350 nm associated with the presence of aromatic rings (PEDOT) gradually increased until 84 h, indicating an accelerated erosion process (Fig. 2c). The eroded product displayed the same absorption curve as pristine PEDOT–COOH in DMSO (Fig. S4†), confirming that the polymer was dissolving into the buffer solution.

To further understand the bioerosion process, we characterized the erosion products in PBS. We first collected and analyzed the solution using FTIR spectroscopy (Fig. S5†). A stretching vibration band around 3350–3500 cm^{-1} assigned to –OH was observed for the pristine polymer. With an increase in incubation time, the

eroded products exhibited characteristic bands of the PEDOT backbone at 1184 cm^{-1} and 1517 cm^{-1} (C–O and C=C), and a carboxyl group at 1705 cm^{-1} (–C=O) with decreased signals for –OH. The almost identical FTIR curves revealed that the eroded product was generated by the dissolving polymer. The change in the surface morphology of PEDOT–COOH residual pellets was investigated by SEM (Fig. 2c). The pellet surface was even and uniform prior to incubation. After 3 days of erosion, the pellet experienced substantial weight loss, resulting in cracks. Several cavities were observed after 5 days due to the severe delamination of PEDOT–COOH particles. These results verify that surface erosion mediated the overall degradation of the PEDOT–COOH pellet.

Cytocompatibility is a prerequisite for biodegradable batteries. After confirming that the eroded products comprised PEDOT–COOH polymeric chains, we first assessed the cytotoxicity of eroded solutions at various concentrations to human adipose-derived stem cells (hADSCs) using 3-[4,5-dimethylthiazol-2-yl]-2,5 diphenyl tetrazolium bromide (MTT) assay. It is noted that a trace amount (<60 μg mL^{-1}) of eroded solutions could promote cell growth (Fig. 2d). Although the cell viability dropped as the concentration of eroded solution increased, overall cell viability was always greater than 80% over a three day incubation, indicating the low cytotoxicity of eroded products.

We further assessed the suitability of the polymer films as substrates for cell adhesion by cultivating hADSCs on a PEDOT–COOH film with a PVA–Au substrate as the control. As the optical

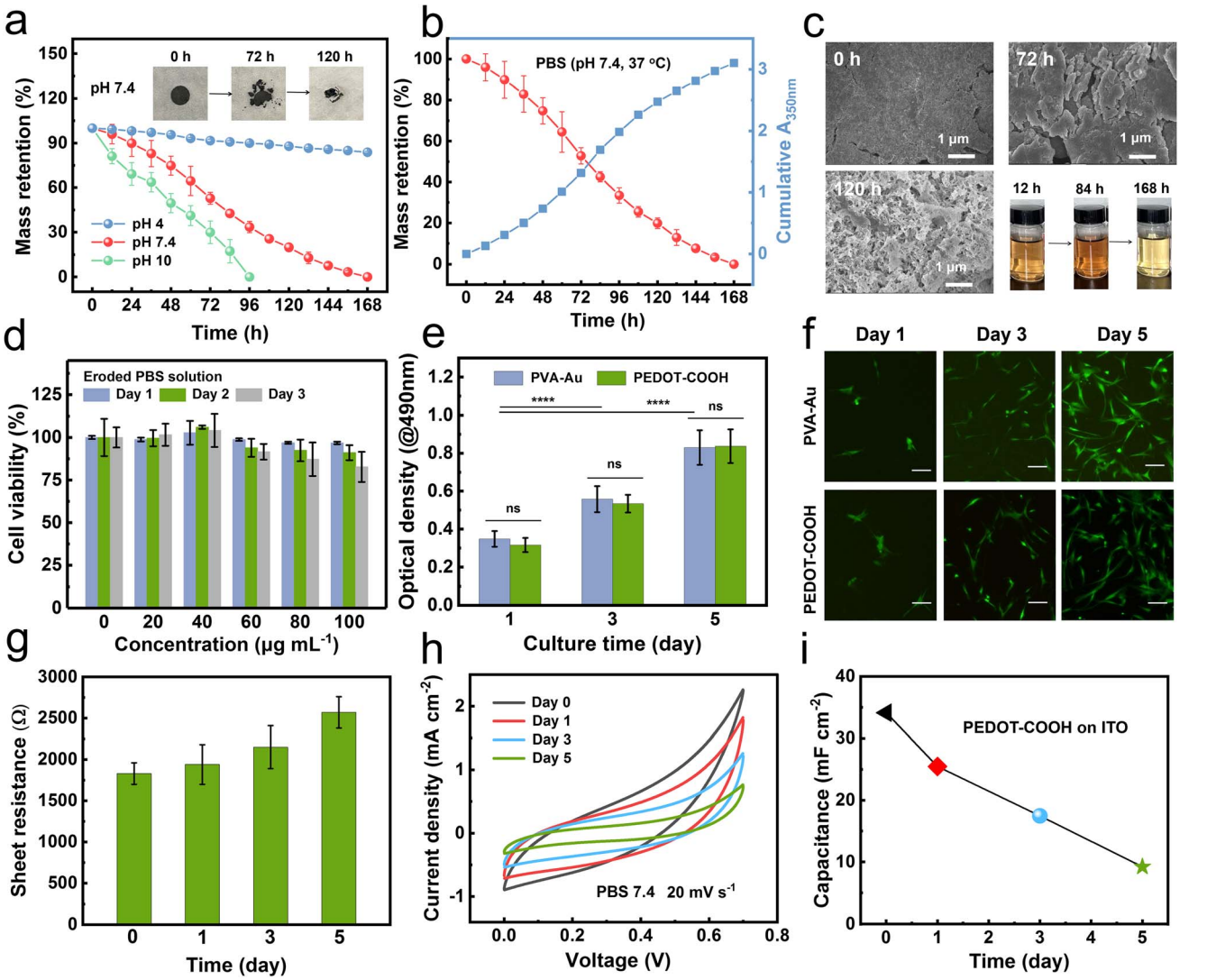

Fig. 2 Bioerosion of PEDOT–COOH pellets in PBS buffers at 37 °C. (a) Mass retention in various pH PBS buffers, and inset shows the optical images of the pellet during the incubation in pH 7.4 PBS solution. (b) Mass retention of the pellet and cumulative absorbance of the eroded solution in pH 7.4 PBS solution. (c) SEM of the pellet before (0 h) and during the incubation (72 h and 120 h). Inset shows the optical images of the eroded solution for 12 h, 84 h, and 168 h. (d) Cell viability of hADSCs cultured with various concentrations of PEDOT–COOH eroded solution for 3 days. (e) Cell proliferation and (f) fluorescence images cultured on PEDOT–COOH and PVA–Au films; scale bar: 100 μm. (g) Electrical conductivity and (h) CV curves at a scan rate of 20 mV s^{-1} of the PEDOT–COOH thin film on ITO during the incubation in pH 7.4 PBS solution. (i) Specific capacitance changes of the PEDOT–COOH thin film on ITO in pH 7.4 PBS solution.

density (OD) value is directly proportional to the number of cells, and the OD value would represent the cell number. The cell proliferation increased as the time elapsed for both samples (Fig. 2e). The cell growth trend of PEDOT–COOH was similar to that of the control over 5 days of incubation, with no statistical difference in cell numbers as evidenced by the similar OD values. Calcein-AM and propidium iodide staining indicated high cell viability in those samples (Fig. 2f). hADSCs spread well and displayed a regular spindle shape and demonstrated good cell proliferation with much higher cell confluency during the three day culture. It is probably attributed to the hydrophilic nature of PEDOT–COOH, providing an adequate surface for cell adhesion.

Taken together, the cell proliferation and minimal cytotoxicity of both the polymer film and eroded products confirmed the compatibility of the PEDOT–COOH substrate.

The effect of bioerosion on the electrical and electrochemical properties was monitored during the incubation period in PBS solution. The electrical conductivity of the pristine PEDOT–COOH thin film on ITO was 1.8 S cm^{-1} measured by a four-point probe method (Fig. 2g). This conductivity was on par with literature values for β-substituted PEDOT.[23] Due to the surface roughness caused by the erosion, we only monitored the sheet resistance during incubation in PBS. The sheet resistance (1800 $\pm$ 80 Ω) increased slightly and reached a plateau of 2530 $\pm$ 260 Ω after 5 days. This equilibrated resistance was similar to that of previously reported functionalized PEDOT used to stimulate cells and tissues in cell culture media.[24]

The cyclic voltammograms (CV) of the PEDOT–COOH film on ITO demonstrated a quasi-rectangular shape without a prominent redox peak in PBS solution (Fig. 2h), indicating high pseudocapacitive activity. Throughout the incubation period, CV profiles were maintained but with a smaller current response. After five days of incubation, a 73% decrease in the specific areal capacitance (9.2 mF cm^{-2}) was observed (Fig. 2i), while the weight loss was 79% at this stage. The decrease in electrochemical activity may be attributed to the disruption of the continuous conductive PEDOT framework caused by surface erosion. The PEDOT–COOH film could maintain electrical and electrochemical activity during erosion under aqueous conditions. Then, after it has fulfilled the function, faster erosion induces rapid mass loss, leading to functional failure.

Electrochemistry of PEDOT–COOH

Zn has been selected as the sacrificial anode for biodegradable batteries due to its high theoretical capacity, acceptable dissolution rate, and favorable biocompatibility.[25] A compact Zn battery was fabricated with an edible gelatin–$ZnSO_4$ gel electrolyte (Fig. 3a). We first investigated the charge storage kinetics of PEDOT–COOH electrodes at various scan rates. The capacitive contribution values (Fig. S6†) were from 86% to 93.5% in the scan rate range of 2 to 10 mV s^{-1}. Such a high surface-controlled contribution reflects the fast kinetics of the PEDOT–COOH electrode.[26] The quasi-rectangular-shaped CV curves at various scan rates suggested good charge storage behavior (Fig. 3b). The electrochemical performance was further revealed by electrochemical impedance spectroscopy (EIS) using Randle's type circuit model (Fig. 3c and S7†). The low bulk resistance (R_s) of 11 Ω, as revealed by the intercept of the Nyquist plot on the real axis reflects good electrical contact and low internal resistance. It also exhibited a charge transport resistance (R_{ct}) of 425 Ω and a 70° line in the low-frequency region, evidencing capacitive behaviors.

Galvanostatic charge–discharge (GCD) profiles demonstrated an almost symmetric and linear shape, implying a small intrinsic series resistance and fast charge–discharge process. The Zn battery delivered a specific capacity of 31.8 to 16.4 mA h g^{-1} at discharge densities from 0.25 to 10 A g^{-1} (Fig. 3d). The specific capacity of PEDOT–COOH at 0.25 A g^{-1} was 57% of its theoretical capacity (55.3 mA h g^{-1} based on a doping level of 0.5 electrons per monomer unit). Attributed to the pseudocapacitance-controlled process of the PEDOT–COOH cathode, the battery exhibited an excellent capacity retention rate (51.5%) at a high 10 A g^{-1} (Fig. 3e). When the current density was reverted to 0.25 A g^{-1}, the initial capacity was nearly restored, demonstrating excellent reversibility. The pseudocapacitance from the conducting polymer backbone endowed the cathode with fast kinetics. Moreover, 78% of the capacity was retained after 4000 cycles at 0.5 A g^{-1}, with a high coulombic efficiency of ~98% (Fig. 3f). The surface morphology of the Zn anode was observed by using a scanning electron microscope (SEM). After long-term cycling, the surface was dense and flat without sharp dendrites (Fig. S8†), indicating the good stability of the Zn anode interfaced with the gel electrolyte.[27] The Zn battery delivered a maximum areal energy density of 39 mW h g^{-1} at a power density of 307 mW g^{-1} (Fig. S9†). Generally, the power requirements for implantable medical devices fall in the range of micro- to milli-watts.[28] These results demonstrate the potential of this rechargeable Zn battery as a viable alternative for powering implantable bioelectronics.

The fact that PEDOT–COOH can be charged and discharged is attributed to the doping/de-doping process in which anions in solution are transferred through the polymer film. To reveal the electrochemical reaction mechanism of the polymer electrodes, the binding energy of S 2p and Zn 2p at various charging/discharging states was analyzed by *ex situ* X-ray photoelectron spectroscopy (XPS, Fig. 3g). In the S 2p region, the peak intensity of the SO_4^{2-} anion ($2p_{1/2}$, 169.5 eV; $2p_{3/2}$, 168.3 eV) during the charging process became stronger, proving the insertion of the SO_4^{2-} anion. Meantime, the high binding energy in PEDOT ($2p_{1/2}$, 165.5 eV; $2p_{3/2}$, 164.3 eV) during the charging process remained constant. The doping level calculated from the peak area ratio of SO_4^{2-} to PEDOT changed from 11.7% (0.95 V) to 20.0% (1.65 V) and then returned to 12.9% (0.95 V) (Fig. S10†), demonstrating a reversible doping–dedoping process. This doping level was similar to that of conventional polythiophene (0.25 holes per monomer ring) used for rechargeable batteries.[29] As for the Zn element, Zn element residuals were observed, probably due to the binding of electrolytes. However, the peak intensity of Zn 2p (1044.9 eV and 1021.9 eV) was almost unchanged during the entire charging/discharging process. The above results rule out the migration of Zn^{2+} in PEDOT–COOH during the electrochemical processes. To investigate if H^+ was involved in the electrochemical reaction, *ex situ* Raman and XRD characterization techniques were carried out during the charging/discharging process (Fig. S11†). Raman spectra displayed similar curve patterns at different

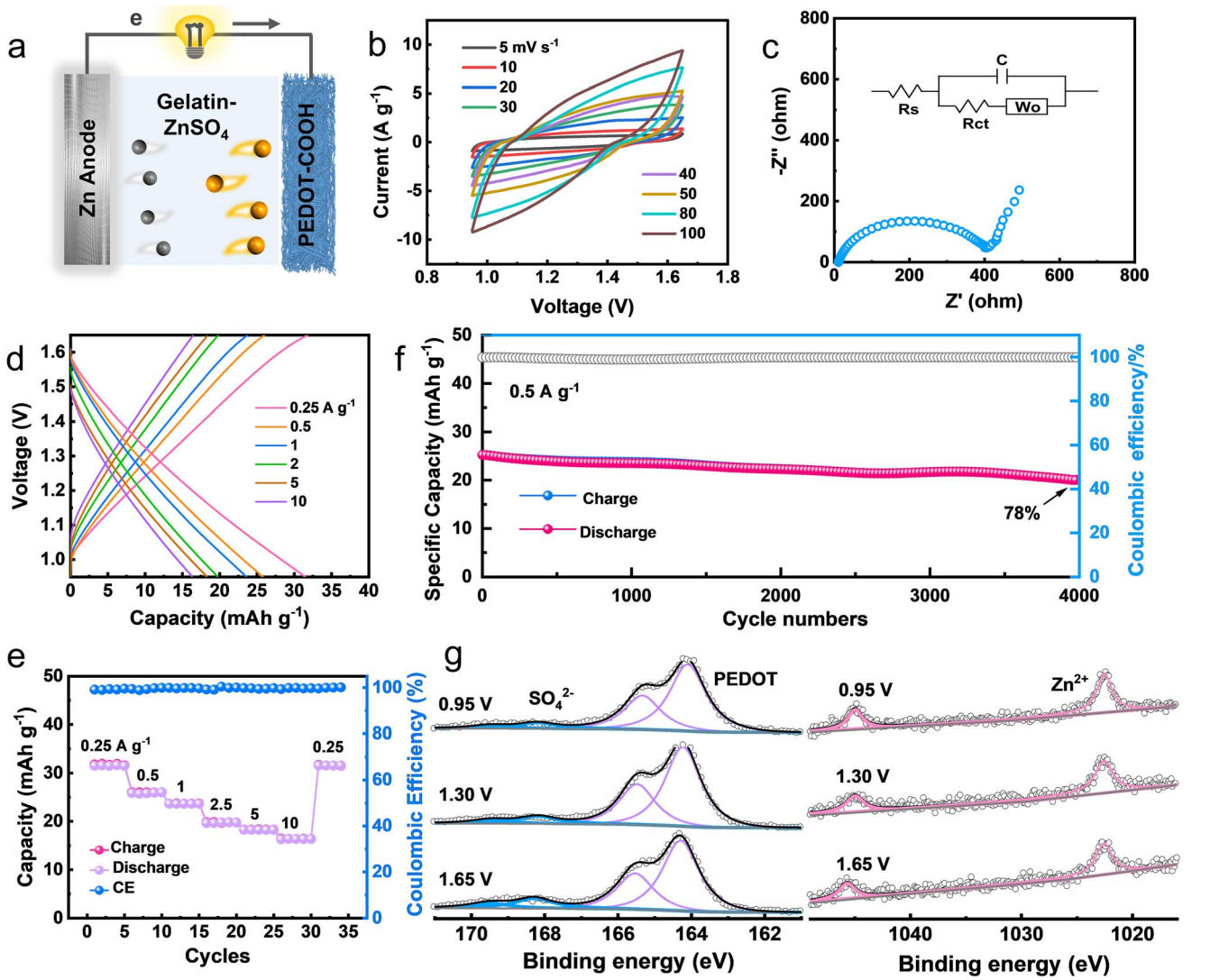

Fig. 3 Electrochemical performance of the Zn battery. (a) Scheme of the battery structure. (b) CV curves at various scan rates. (c) Nyquist plots with the equivalent circuit used for the simulation. (d) GCD curves at various current densities. (e) Rate performance and coulombic efficiency. (f) Capacity retention after 4000 cycles at 0.5 A g^{-1}. (g) The *ex situ* XPS spectra of the S 2p and Zn 2p regions of PEDOT–COOH.

charging stages. The peak intensity of SO_4^{2-} at 575 and 980 cm^{-1} continued to increase from 0.95 V to 1.65 V, evidencing the insertion during the charging process. No peak for zinc sulfate hydroxide hydrate (ZHS) can be identified in the Raman and XRD patterns, which may exclude the proton insertion during the charging/discharging process.[30,31] In this Zn–polymer battery system, during the charging process, Zn^{2+} was transferred and reduced on the anode side, while SO_4^{2-} anions were inserted into the backbone of PEDOT. During discharging, Zn was oxidized and migrated in the electrolyte as Zn^{2+}, whereas the reduction of PEDOT led to the expulsion of the dopants. The main electrochemical reactions were as follows:

At the anode:

$$Zn + SO_4^{2-} \leftrightarrow ZnSO_4 + 2e^-$$

At the cathode:

$$2(PEDOT–COOH)^+/SO_4^{2-} + 2e^- \leftrightarrow 2(PEDOT–COOH)^0 + SO_4^{2-}$$

Overall reaction:

$$Zn + 2(PEDOT–COOH)^+/SO_4^{2-} \leftrightarrow 2(PEDOT–COOH)^0 + ZnSO_4$$

Implantation of the Zn battery

We fabricated a small-sized and lightweight Zn–polymer battery (thickness of 1000 μm and weight of 300 mg) using PVA substrates encapsulated by thermal processing. We used Joule heating treatment to program the crystallinity of the PVA

substrate, resulting in a decreased swelling rate and slow dissolution time.[32] The battery consisted of a Zn foil anode (10 μm, 5 mg), edible gelatin–$ZnSO_4$ gel electrolyte (90 μm, 25 mg), PEDOT–COOH cathode on a PVA–Au electrode (100 μm, 30 mg), and PVA packaging (800 μm, 240 mg). Generally, the Zn element is found at 20–35 mg kg^{-1} for adults, with a recommended daily allowance of 40 mg.[33] Fig. 4a illustrates the degradation process of the encapsulated battery in PBS solution at various stages. The outer PVA encapsulation layer degraded first, followed by the disintegration of the biodegradable battery. The gel electrolyte and PVA substrate were completely dissolved within 7 days. However, Zn foil took another 23 days to disappear completely at an elevated temperature (85 °C). Generally, the Zn film degraded *in vitro* at a rate of 0.3 ± 0.2 μm h^{-1} in Hank's solution at pH 7.4 at 37 °C.[34] The Au component (0.29 mg/300 mg device) was physically fragmented *in vivo* because of the degradation of the PVA substrate. Au nanoparticles are considered non-toxic with an appropriate size and dosage, and metabolization occurs through the kidney, bladder, or hepatobiliary system.[35]

The encapsulated battery was implanted in the dorsal subcutaneous region of SD rats. Since the PVA substrate made up the majority of the battery by mass, it predominantly dictated the degradation process of the device. The external packaging layer was fully resorbed by the SD rat through metabolism after four weeks, along with the leakage of Zn flakes and the PEDOT–COOH film from the edges of the broken implant (Fig. 4b). Traces of the battery components could be observed in the subdermal region after six weeks, followed by their complete disappearance after eight weeks. The *in vivo* degradation rate was slower than *in vitro*, attributed to the dynamic environment in the animal body.[36] To investigate the effects of biodegradation on the organism, the dorsal tissue close to the implantation sites and major organs were stained with hematoxylin and eosin (H&E) during the biodegradation (Fig. 4c). After four weeks, no obvious macrophage aggregation or inflammatory response was observed, suggesting their biocompatibility. Moreover, the batteries demonstrated negligible toxicity and side effects after eight weeks of complete degradation, as revealed by the H&E staining of main organs such as the heart, liver, spleen, lung, and kidney. The *in vitro* and *in vivo* experiments demonstrate the biocompatibility of the battery over the whole life, which was derived from the non-toxic nature of constituent materials and degradation byproducts. Taken together, this polymer-based Zn battery delivered a high output voltage (1.2 V) and high capacity retention at a high rate (51.5%, 10 A g^{-1}). Moreover, it displayed a full biodegradation profile in PBS after 30 days or 56 days *in vivo*, in contrast to previously reported biodegradable implanted batteries where unreacted active components such as MnO_2 and carbon electrodes were left in PBS or *in vivo* (Table S1†).[37–40]

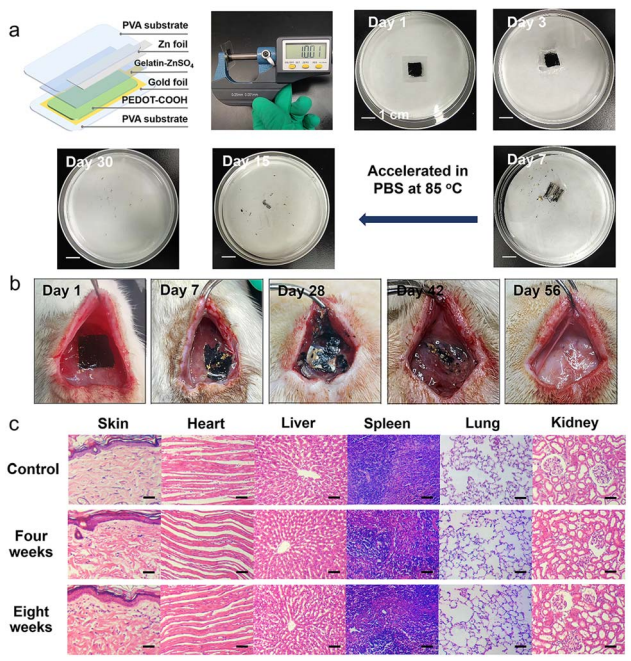

Fig. 4 Biodegradation and biocompatibility assessment of the implantable Zn battery. (a) Scheme and photographs of the time-sequential erosion in PBS solution. (b) Photographs of the *in vivo* biodegradation evaluation in the subcutaneous area of SD rats. (c) H&E staining of subcutaneous tissues close to the implantation site and major organs with and without implantation; scale bar: 50 μm.

Conclusions

In this work, we have synthesized a fully erodible conducting polymer for an implanted rechargeable battery. Side-chain engineering of a hydrolysable carbonyl group endows the functionalized PEDOT with desirable full erosion after seven days of incubation in PBS solution while maintaining an extended π-conjugation backbone. The polymer could preserve its electrical conductivity in PBS throughout five days of exposure. The electropolymerized film promotes the adhesion and proliferation of hADSCs without causing cytotoxicity in the degraded products. The rechargeable Zn battery exhibits outstanding cycling stability. Evaluation in subcutaneous implantation of the Zn battery demonstrates full biodegradation and no detectable toxic effect of the constitutional material or its degraded product. This erodible PEDOT may find future applications as temporary scaffolds for the electro-stimulation of cells and transient electronic-tissue interfaces.

Ethical statement

All *in vivo* experiments were approved by the Institutional Animal Care and Use Committee (IACUC) of Jilin University (Approval No. 2022-0599).

Data availability

All the data in this study are available in the manuscript or ESI.† Correspondence and requests for materials should be addressed to the corresponding authors.

Author contributions

X. Jia: investigation, methodology, formal analysis, and writing-original draft; X. Ma: methodology, investigation, and

formal analysis; L. Zhao: investigation and methodology; M. Xin: methodology and formal analysis; Y. Hao: resources and formal analysis; P. Sun: data curation; C. Wang: software. D. Chao: conceptualization and methodology; F. Liu: resources and supervision. C. Wang: conceptualization, methodology, and writing-review & editing; G. Lu: project administration and funding acquisition; G. Wallace: conceptualization and writing-review & editing.

Conflicts of interest

There are no conflicts to declare.

Acknowledgements

This work is supported by the National Natural Science Foundation of China (521032089, 62122030, and 22275066) and Jilin Provincial Science and Technology Department (20210508046RQ). C. Wang and G. Wallace acknowledge the support from the Australian Research Council Centre of Excellence Scheme (CE 140100012).

References

1 C. Li, C. Guo, V. Fitzpatrick, A. Ibrahim, M. J. Zwierstra, P. Hanna, A. Lechtig, A. Nazarian, S. J. Lin and D. L. Kaplan, *Nat. Rev. Mater.*, 2020, **5**, 61.
2 H. Sheng, X. Zhang, J. Liang, M. Shao, E. Xie, C. Yu and W. Lan, *Adv. Healthcare Mater.*, 2021, **10**, 2100199.
3 X. Jia, C. Wang, C. Y. Lee, C. Yu and G. G. Wallace, *MRS Bull.*, 2020, **45**, 121.
4 S. Y. Yang, V. Sencadas, S. S. You, N. Z. X. Jia, S. S. Srinivasan, H. W. Huang, A. E. Ahmed, J. Y. Liang and G. Traverso, *Adv. Funct. Mater.*, 2021, **31**, 2009289.
5 X. Jia, C. Wang, V. Ranganathan, B. Napier, C. Yu, Y. Chao, M. Forsyth, F. G. Omenetto, D. R. MacFarlane and G. G. Wallace, *ACS Energy Lett.*, 2017, **2**, 831.
6 M. Karami-Mosammam, D. Danninger, D. Schiller and M. Kaltenbrunner, *Adv. Mater.*, 2022, **34**, 2204457.
7 Y. Jang, T. Park, E. Kim, J. W. Park, D. Y. Lee and S. J. Kim, *Angew. Chem., Int. Ed.*, 2021, **60**, 10563–10567.
8 Y. J. Kim, A. Khetan, W. Wu, S. E. Chun, V. Viswanathan, J. F. Whitacre and C. J. Bettinger, *Adv. Mater.*, 2016, **28**, 3173–3180.
9 T. Mei, C. Wang, M. Liao, J. Li, L. Wang, C. Tang, X. Sun, B. Wang and H. Peng, *J. Mater. Chem. A*, 2021, **9**, 10104–10109.
10 N. Mittal, A. Ojanguren, M. Niederberger and E. Lizundia, *Adv. Sci.*, 2021, **8**, 2004814.
11 X. Jia, Y. Ge, L. Shao, C. Wang and G. G. Wallace, *ACS Sustainable Chem. Eng.*, 2019, **7**, 14321–14340.
12 V. R. Feig, H. Tran and Z. Bao, *ACS Cent. Sci.*, 2018, **4**, 337–348.
13 T. J. Rivers, T. W. Hudson and C. E. Schmidt, *Adv. Funct. Mater.*, 2002, **12**, 33.
14 T. Lei, M. Guan, J. Liu, H. C. Lin, R. Pfattner, L. Shaw, A. F. McGuire, T. C. Huang, L. Shao, K. T. Cheng, J. B. H. Tok and Z. Bao, *Proc. Natl. Acad. Sci. U. S. A.*, 2017, **114**, 5107–5112.
15 H. Tran, V. R. Feig, K. Liu, H. C. Wu, R. Chen, J. Xu, K. Deisseroth and Z. Bao, *ACS Cent. Sci.*, 2019, **5**, 1884–1891.
16 J. A. Chiong, Y. Zheng, S. Zhang, G. Ma, Y. Wu, G. Ngaruka, Y. Lin, X. Gu and Z. Bao, *J. Am. Chem. Soc.*, 2022, **144**, 3717–3726.
17 D. Mawad, A. Artzy-Schnirman, J. Tonkin, J. Ramos, S. Inal, M. M. Mahat, N. Darwish, L. Zwi-Dantsis, G. G. Malliaras, J. J. Gooding, A. Lauto and M. M. Stevens, *Chem. Mater.*, 2016, **28**, 6080–6088.
18 E. M. Ali, E. A. B. Kantchev, H. H. Yu and J. Y. Ying, *Macromolecules*, 2007, **40**, 6025.
19 C. Baker, K. Wagner, P. Wagner, D. L. Officer and D. Mawad, *Adv. Phys.: X*, 2021, **6**, 1899850.
20 D. Mawad, K. Gilmore, P. Molino, K. Wagner, P. Wagner, D. L. Officer and G. G. Wallace, *J. Mater. Chem.*, 2011, **21**, 5555.
21 A. N. Zelikin, D. M. Lynn, J. Farhadi, I. Martin, V. Shastri and R. Langer, *Angew. Chem., Int. Ed.*, 2002, **41**, 141–144.
22 J. A. Chiong, H. Tran, Y. Lin, Y. Zheng and Z. Bao, *Adv. Sci.*, 2021, **8**, 2101233.
23 H. Shi, C. Liu, Q. Jiang and J. Xu, *Adv. Electron. Mater.*, 2015, **1**, 1500017.
24 D. Minudri, D. Mantione, A. Dominguez-Alfaro, S. Moya, E. Maza, C. Bellacanzone, M. R. Antognazza and D. Mecerreyes, *Adv. Electron. Mater.*, 2020, **6**, 2000510.
25 N. Dong, F. Zhang and H. Pan, *Chem. Sci.*, 2022, **13**, 8243–8252.
26 Y. Dai, X. Liao, R. Yu, J. Li, J. Li, S. Tan, P. He, Q. An, Q. Wei, L. Chen, X. Hong, K. Zhao, Y. Ren, J. Wu, Y. Zhao and L. Mai, *Adv. Mater.*, 2021, **33**, 2100359.
27 X. Zhou, Q. Zhang, Z. Hao, Y. Ma, O. A. Drozhzhin and F. Li, *ACS Appl. Mater. Interfaces*, 2021, **13**, 53227.
28 S. K. Kang, J. Koo, Y. K. Lee and J. A. Rogers, *Acc. Chem. Res.*, 2018, **51**, 988–998.
29 S. Muench, A. Wild, C. Friebe, B. Häupler, T. Janoschka and U. S. Schubert, *Chem. Rev.*, 2016, **116**, 9438–9484.
30 Y. Liu, X. Lu, F. Lai, T. Liu, P. R. Shearing, I. P. Parkin, G. He and D. J. L. Brett, *Joule*, 2021, **5**, 2845–2903.
31 M. R. Tuttle, C. Walter, E. Brackman, C. E. Moore, M. Espe, C. Rasik, P. Adams and S. Zhang, *Chem. Sci.*, 2021, **12**, 15253–15262.
32 Z. Wang, Q. Lu, Y. Xia, S. Feng, Y. Shi, S. Wang, X. Yang, Y. Zhao, F. Sun, T. Li and T. Zhang, *Microsyst. Nanoeng.*, 2021, **7**, 56.
33 C. J. Bettinger, *Trends Biotechnol.*, 2015, **33**, 575–585.
34 L. Yin, H. Cheng, S. Mao, R. Haasch, Y. Liu, X. Xie, S. W. Hwang, H. Jain, S. K. Kang, Y. Su, R. Li, Y. Huang and J. A. Rogers, *Adv. Funct. Mater.*, 2014, **24**, 645–658.
35 M. Longmire, P. L. Choyke and H. Kobayashi, *Nanomedicine*, 2008, **3**, 703.
36 G. Yao, L. Kang, C. Li, S. Chen, Q. Wang, J. Yang, Y. Long, J. Li, K. Zhao, W. Xu, W. Cai, Y. Lin and X. Wang, *Proc. Natl. Acad. Sci. U. S. A.*, 2021, **118**, e2100772118.

37 J. Zhou, R. Zhang, R. Xu, Y. Li, W. Tian, M. Gao, M. Wang, D. Li, X. Liang, L. Xie, K. Liang, P. Chen and B. Kong, *Adv. Funct. Mater.*, 2022, **32**, 2111406.
38 Y. Zhao, T. Mei, L. Ye, Y. Li, L. Wang, Y. Zhang, P. Chen, X. Sun, C. Wang and H. Peng, *J. Mater. Chem. A*, 2021, **9**, 1463–1470.
39 M. H. Lee, J. Lee, S. K. Jung, D. Kang, M. S. Park, G. D. Cha, K. W. Cho, J. H. Song, S. Moon, Y. S. Yun, S. J. Kim, Y. W. Lim, D. H. Kim and K. Kang, *Adv. Mater.*, 2021, **33**, 2004902.
40 T. P. Nguyen, A. D. Easley, N. Kang, S. Khan, S. M. Lim, Y. H. Rezenom, S. Wang, D. K. Tran, J. Fan, R. A. Letteri, X. He, L. Su, C. H. Yu, J. L. Lutkenhaus and K. L. Wooley, *Nature*, 2021, **593**, 61–66.